1-1-2014

# Mixed Quantum/Classical Calculations of Total and Differential Elastic and Rotationally Inelastic Scattering Cross Sections for Light and Heavy Reduced Masses in a Broad Range of Collision Energies

Alexander Semenov
*Marquette University*

Dmitri Babikov
*Marquette University*, dmitri.babikov@marquette.edu

Published version. *Journal of Chemical Physics*, Vol. 140 (2014): 044306: 1-13. DOI. 

# Mixed quantum/classical calculations of total and differential elastic and rotationally inelastic scattering cross sections for light and heavy reduced masses in a broad range of collision energies

Alexander Semenov and Dmitri Babikov[a)]
*Chemistry Department, Wehr Chemistry Building, Marquette University, Milwaukee, Wisconsin 53201-1881, USA*

(Received 27 November 2013; accepted 5 January 2014; published online 23 January 2014)

The mixed quantum/classical theory (MQCT) for rotationally inelastic scattering developed recently [A. Semenov and D. Babikov, J. Chem. Phys. **139**, 174108 (2013)] is benchmarked against the full quantum calculations for two molecular systems: He + $H_2$ and Na + $N_2$. This allows testing new method in the cases of light and reasonably heavy reduced masses, for small and large rotational quanta, in a broad range of collision energies and rotational excitations. The resultant collision cross sections vary through ten-orders of magnitude range of values. Both inelastic and elastic channels are considered, as well as differential (over scattering angle) cross sections. In many cases results of the mixed quantum/classical method are hard to distinguish from the full quantum results. In less favorable cases (light masses, larger quanta, and small collision energies) some deviations are observed but, even in the worst cases, they are within 25% or so. The method is computationally cheap and particularly accurate at higher energies, heavier masses, and larger densities of states. At these conditions MQCT represents a useful alternative to the standard full-quantum scattering theory.
 [http://dx.doi.org/10.1063/1.4862409]

## I. INTRODUCTION

The main goal of this paper is to explore the limits of validity of the mixed quantum/classical theory (MQCT) for rotationally inelastic atom + molecule scattering.[1]

Foundations of MQCT were laid by Gert Billing in 1980s, but the main body of his work belongs to *vibrationally inelastic* scattering and development of the method in which vibration of the molecule is treated quantum mechanically, while its rotation and the scattering process are treated classically.[2,3] In recent years such methods have been revived and improved,[4–6] and applied to complicated problems, such as recombination reactions.[7–9]

For description of *rotationally inelastic* scattering Billing proposed another version of MQCT, in which the rotational motion is treated quantum mechanically, and only the translational motion is treated classically.[2,3] He applied this theory to one system, He + $H_2$, at two relatively high values of scattering energies: $E = 0.1$ and 0.9 eV.[10] Those ground-breaking results were included into a review paper[2] and a book[3] but, surprisingly, remained the only example of MQCT treatment of rotationally inelastic scattering.

Detailed analysis of Billing's work reveals that he employed only an approximate version of MQCT, known as coupled-states (CS) approximation, where transitions between different $m$-states, within the same rotational energy level $j$, are entirely neglected. We also found that the equations Billing used are applicable only to the simplest case, when the initial rotational wave function has cylindrical symmetry (i.e., describes pure eigenstate). Such equations cannot be employed to handle a general case, when the initial rotational wave function corresponds to an arbitrary superposition of eigenstates (a wave packet).

In a recent theory paper[1] we presented a general and fully coupled version of MQCT for rotationally inelastic scattering, formulated in both laboratory-fixed and body-fixed (BF) reference frames and tested it using a model system. Here we present results of calculations for two real systems, Na + $N_2$ and He + $H_2$, carried out in a broad range of scattering energies. For our best knowledge this is the first systematic and rigorous study of MQCT for rotationally inelastic scattering. Our choice of the benchmark systems was based on the following arguments. First of all, accurate full-quantum coupled-channel (CC) results for these systems are available from recent literature,[11–13] as well as potential energy surfaces (PES) used in those studies. Second, all atoms in Na + $N_2$ are relatively heavy, while they are light in the He + $H_2$. This gives opportunity to observe the effect of reduced mass of the scattering partners – an important aspect for the method where scattering is treated classically. Third, the rotational quanta in heavy $N_2$ and light $H_2$ are very different, spanning the range of transition energies $\Delta E$ from $\sim$12 cm$^{-1}$ to $\sim$813 cm$^{-1}$, which allows testing applicability of second Delos criterion.[14] Namely, based on this criterion, it is sometimes argued that any mixed quantum/classical method is accurate only when the classical collision energy $E$ is much larger than the energy change $\Delta E$ associated with quantum transition between the internal states.[14] However, for MQCT treatment of rotationally inelastic scattering this criterion has never been tested and our results indicate that MQCT remains accurate in a broader range than predicted by this criterion.

[a)]Author to whom correspondence should be addressed. Electronic mail: dmitri.babikov@mu.edu

 

Another aspect that, to our best knowledge, has not been addressed before within MQCT framework is calculation of the elastic scattering cross section and the differential (over scattering angle) cross section. It is well known that classical scattering theory is deficient in these two respects. At large impact parameters and small scattering angles the classical scattering cross section diverges, due to the lack of phase information. Only at scattering angles larger than the "rainbow" angle (small impact parameters) the process of scattering is classical. Interestingly, we found a way to compute the scattering phase using MQCT, and use it to compute accurate differential cross section at small scattering angles, i.e., in the quantum scattering regime when interference is important.

The paper is organized as follows: In Sec. II we review major equations of the fully coupled general MQCT, its simplified version, and the approximate CS version and also present the method of computing cross sections. In Sec. III we report numeric results for the integral rotationally inelastic scattering cross sections for two benchmark systems and compare them with full quantum CC results, as well as with complementary classical trajectory simulations, in a broad range of collision energies. Section IV is devoted to elastic scattering cross sections and differential cross sections computed by MQCT. Major findings are summarized in Sec. V.

## II. THEORETICAL FRAMEWORK

### A. General and fully coupled MQCT

From the computational performance point of view the most efficient formulation of MQCT is that in the BF reference frame.[1] In order to simplify notations, in this paper we use $jm$ and $j'm'$ to label the initial and final rotational sates of the molecule, instead of $j'm'$ and $j''m''$ used in Ref. 1, and we also use $\varphi$ instead of $\varphi'$ used in Ref. 1. Rotational and vibrational motion of the diatomic molecule is described by coordinates $\mathbf{q} = (r, \gamma, \varphi)$. These are quantum degrees of freedom; their evolution is determined by wave function $\psi(r, \gamma, \phi)$. Scattering of the quencher atom is described by spherical polar coordinates $\mathbf{Q} = (R, \Theta, \Phi)$. These are classical degrees of freedom; their evolution is determined by conjugate momenta $P_R$, $P_\Theta$, and $P_\Phi$. Interaction potential does not depend on classical angles and angle $\varphi$ due to symmetry, so, potential is a function of Jacobi variables $V = V(R, r, \gamma)$. Definition of these coordinates in the BF reference frame is illustrated in Fig. 2 of Ref. 1. The MQCT equations of motion for classical variables are:[1]

$$\dot{R} = \frac{P_R}{\mu}, \tag{1}$$

$$\dot{\Theta} = \frac{P_\Theta}{\mu R^2}, \tag{2}$$

$$\dot{\Phi} = \frac{P_\Phi}{\mu\, R^2 \sin^2\Theta}, \tag{3}$$

$$\dot{P}_R = -\frac{\partial \tilde{V}(R)}{\partial R} + \frac{P_\Theta^2}{\mu\, R^3} + \frac{P_\Phi^2}{\mu\, R^3 \sin^2\Theta}, \tag{4}$$

$$\dot{P}_\Theta = \sum_{n'j'm'} \sum_{njm} a^*_{n'j'm'} a_{njm} \exp\{i(E_{n'j'} - E_{nj})t/\hbar\} \times [\mathbf{M}, \mathbf{U}]^{n'j'm'}_{njm} + \frac{P_\Phi^2 \cos\Theta}{\mu\, R^2 \sin^3\Theta}, \tag{5}$$

$$\dot{P}_\Phi = -i \sum_{n'j'm'} \sum_{njm} a^*_{n'j'm'} a_{njm} \times \exp\{i(E_{n'j'} - E_{nj})t/\hbar\} \sin\Theta\, [\mathbf{M}, \mathbf{V}]^{n'j'm'}_{njm}. \tag{6}$$

Here we introduced the mean-field potential $\tilde{V}(R) = \langle \psi(r, \gamma, \varphi) | V(R, r, \gamma) | \psi(r, \gamma, \varphi) \rangle$ and the commutators [**M**,**U**] and [**M**, **V**] of the matrices introduced below. Expansion of wave function over the basis set of rovibrational eigenstates with time-dependent coefficients $a_{njm}(t)$ and substitution into Schrodinger equation leads to:[1]

$$i\hbar \frac{\partial a_{njm}}{\partial t} = \sum_{n'j'} a_{n'j'm} \exp\{i(E_{nj} - E_{n'j'})t/\hbar\} \times M^{n'j'}_{nj}(R) - i\hbar \sum_{m'} a_{njm'} W^{m'}_{m}. \tag{7}$$

Structure of these coupled equations is such that the state-to-state transition matrix $M^{n'j'}_{nj}$, introduced for every $m$ as

$$M^{n'j'}_{nj}(R) = A_{j'm,jm} \langle \phi_{nj}(r) P_{jm}(\cos\gamma) \times |V(R, r, \gamma)| \phi_{n'j'}(r) P_{j'm}(\cos\gamma) \rangle, \tag{8}$$

describes only transitions from $(n\,j)$ to $(n'j')$, within the same value of $m$. In contrast, the matrix $W^{m'}_{m}$, introduced for every $j$, describes transitions between $m$ and $m' = m \pm 1$, within the same energy level $(n\,j)$. Elements of this matrix,

$$W^{m'}_{m} = U^{m'}_{m}\, \dot{\Theta} + i\, (\sin\Theta V^{m'}_{m} - m' \cos\Theta \delta_{m,m'})\, \dot{\Phi}, \tag{9}$$

are expressed through elements of two simpler matrices:[1]

$$U^{m'}_{m} = \frac{1}{2}\Big[\sqrt{j(j+1) - m'(m'-1)}\,\delta_{m,m'-1} - \sqrt{j(j+1) - m'(m'+1)}\,\delta_{m,m'+1}\Big] \tag{10}$$

and

$$V^{m'}_{m} = \frac{1}{2}\Big[\sqrt{j(j+1) - m'(m'-1)}\,\delta_{m,m'-1} + \sqrt{j(j+1) - m'(m'+1)}\,\delta_{m,m'+1}\Big]. \tag{11}$$

Matrices **M**, **U**, and **V** are all real-valued, sparse, and time-independent (should be computed only once). Note that elements of the matrix **M** and the mean-field potential $\tilde{V}$ depend on $R$ only.

### B. A simplified version of MQCT

If the initial rotational wave function exhibits cylindrical symmetry around the atom-molecule axis (i.e., corresponds to rotational eigenstate, rather than rotational wave packet) the classical trajectory remains in the same plane during the course of entire collision event. In such cases we can restrict our calculations to one plane, for example, $\Theta = \pi/2$ and set $P_\Theta = 0$. Equations (2)–(5) simplify to

$$\dot{\Theta} = 0, \tag{2'}$$

$$\dot{\Phi} = \frac{P_\Phi}{\mu R^2}, \tag{3'}$$

$$\dot{P}_R = -\frac{\partial \tilde{V}(R)}{\partial R} + \frac{P_\Phi^2}{\mu R^3}, \tag{4'}$$

$$\dot{P}_\Theta = 0. \tag{5'}$$

Clearly, Eqs. (2′) and (5′) are obsolete and there is no need to propagate them. Equation (6) becomes

$$\dot{P}_\Phi = -i \sum_{n'j'm'} \sum_{njm} a^*_{n'j'm'} a_{njm} \times \exp\{i(E_{n'j'} - E_{nj})t/\hbar\} [\mathbf{M}, \mathbf{V}]^{n'j'm'}_{njm}. \tag{6'}$$

### C. An approximate CS version of MQCT

The coupled-states (CS) approximation is easily formulated within MQCT by setting $W^{m'}_m = 0$ in Eq. (7) for wave function evolution. It becomes:

$$i\hbar \frac{\partial a_{nj}}{\partial t} = \sum_{n'j'} a_{n'j'} \exp\{i(E_{nj} - E_{n'j'})t/\hbar\} \, M^{n'j'}_{nj}(R), \tag{7'}$$

and should be solved for every value of $m$ separately. Classical equations of motion (5) and (6) also simplify significantly, because the commutator matrices vanish: $[\mathbf{M},\mathbf{U}] = 0$ and $[\mathbf{M}, \mathbf{V}] = 0$. If this CS-approximation is used together with simplification of Sec. II B (cylindrical symmetry), then Eqs. (5) and (6) convert into

$$\dot{P}_\Theta = 0, \tag{5''}$$

$$\dot{P}_\Phi = 0. \tag{6''}$$

Again, these equations are trivial and there is no need to propagate them.

In this form the MQCT becomes rather simple and similar to the method of Billing,[2] with only one distinction. Billing has chosen to restrict his trajectories to $\Phi = 0$ plane and set $P_\Phi = 0$. In principle this is equivalent, but in practice our version is better, because fixing $\Theta = \pi/2$ permits to avoid singularity at $\Theta = 0$, which affects Eqs. (3) and (4), and (5). Equation (1) remains in its original form in any version of MQCT.

### D. Sampling of initial conditions

The exact quantum expressions for (integral) scattering cross section are[15]

$$\sigma_{j\to j'} = \frac{1}{(2j+1)} \sum_{m=-j}^{j} \sum_{m'=-j'}^{j'} \sigma_{jm\to j'm'}, \tag{12}$$

$$\sigma_{jm\to j'm'} = \frac{\pi}{k_j^2} \sum_{J=0}^{\infty} \sum_{l=|J-j|}^{J+j} \sum_{l'=|J-j'|}^{J+j'} (2J+1) \times \left| \delta_{jj'}\delta_{ll'}\delta_{mm'} - S^J_{jj',ll',mm'} \right|^2, \tag{13}$$

where $S^J_{jj',ll',mm'}$ is the scattering matrix in BF system. MQCT treatment is most straightforward for *inelastic* scattering channels, when $\delta_{jj'} = 0$ and the probability amplitudes $a_{j'm'}$ from Eq. (7) at the final moment of time can be used to compute transition probability as $|\delta_{jj'}\delta_{ll'}\delta_{mm'} - S^J_{jj',ll',mm'}|^2 = |a_{j'm'}|^2$. Transformation to MQCT treatment is achieved by making the total angular momentum $J$ a continuous (classical) variable, while keeping the values of $j$ and $m$ integer and quantized. This imposes certain restrictions onto the values of continuous classical variable $\ell = |\mathbf{l}|$, namely: $|J - j| \le \ell \le J + j$. Figure 1 explains sampling of initial conditions, including illustration of the allowed values for classical vector of orbital angular momentum $\mathbf{l}$, related closely to the collision impact parameter $b$ through $\ell(\ell+1) = k^2 b^2$ and $\mathbf{k} = \mathbf{P}/\hbar$. Absolute value of the initial momentum $\mathbf{P}^2 = P_R^2 + (P_\Phi^2 / \sin^2\Theta + P_\Theta^2)/R^2$ is determined by incident energy of collision, while various possible *directions* of $\mathbf{P}$ in space correspond to different values of $\ell = |\mathbf{l}|$, where $\mathbf{l} = \mathbf{J} + \mathbf{j}$. In a general situation (without cylindrical symmetry, $\Theta \neq const$) the range of possible directions of $\mathbf{P}$ is represented by a segment of spherical surface illustrated in Fig. 1. If the simplified version of theory (cylindrical symmetry) is appropriate, this range shrinks to a one-dimensional section of this surface by $\Theta = \pi/2$ plane.

Following these arguments, the triple sum in quantum Eq. (13) is replaced by classical integral:

$$\sigma_{jm\to j'm'} = \frac{\pi}{k_j^2} \int_0^\infty (2J+1) dJ \int_{\mathbf{l}=\mathbf{J}+\mathbf{j}} \left| a_{j'm'} \right|^2 d\mathbf{l}. \tag{14}$$

In practice, this integral is estimated using the Monte-Carlo sampling technique. First, the value of $J$ is sampled randomly

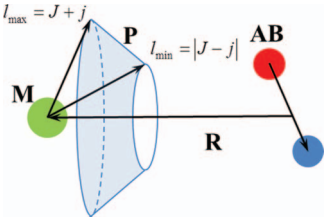


FIG. 1. Sampling of initial conditions for atom-molecule collision in space-fixed (SF) reference frame. Shaded area on the surface of the sphere of radius $|\mathbf{P}|$ determines all possible directions of classical vector $\mathbf{P}$. Different directions correspond to different values of impact parameter, with largest impact parameter obtained in the case of $l_{max}$ and smallest impact parameter in the case of $l_{min}$.

and uniformly between zero and $J_{\max} = k\hbar b_{\max}$. Next, for a chosen initial $j$, the value of $\ell$ is sampled randomly and uniformly in the range $|J - j| \le \ell \le J + j$, and is used to define the initial classical momentum $P_\Phi = \hbar\sqrt{\ell(\ell+1)}$ in Eq. (3)–(5). This procedure is repeated for $N$ classical trajectories (labeled by $i$) and the inelastic scattering integral cross section is determined numerically as

$$\sigma_{jm\to j'm'} = \frac{\pi}{k^2}\frac{J_{\max}}{N}\sum_i (2J^{(i)}+1)\left|a^{(i)}_{j'm'}\right|^2. \quad (15)$$

Quantum equation (12) is used in MQCT without modifications; it describes sum over the final values $m'$ and average over the initial values $m$.

It may also be instructive to consider the trivial case of $j = 0$, when $J = \ell$ and the range of possible directions of vector $P$ shrinks to a single point. In this case no sampling over $\ell$ is needed at all, the integral in Eq. (14) becomes one-dimensional, $\sigma_{jm\to j'm'} = \pi/k_j^2 \int (2J+1)|a_{j'm'}|^2 dJ$, which can be easily evaluated using any structured grid method (no Monte-Carlo needed). However, when $j > 0$, it is advantageous to use the two-dimensional Monte-Carlo sampling over $J$ and $\ell$, for faster convergence.

### E. Phases and elastic scattering cross sections

For the elastic scattering channel the phase of the corresponding diagonal element of scattering matrix $S$ in Eq. (13) becomes important, but there are two contributions to the overall phase. One contribution is phase of rotational (or ro-vibrational, internal) wave function. It is contained in the complex-valued transition amplitude $a_{jm}$, which is accurately computed within MQCT by propagating Eq. (7). We will denote this phase $\delta_j$ and compute it as $\delta_j = \arg a_{jm}$. Second contribution is phase shift of the partial wave, $\delta_\ell$, which is missing in MQCT because scattering is treated classically. However, classical treatment of scattering provides classical deflection function $\Theta(\ell)$. The deflection function cannot really be used directly to compute cross section at angles smaller than the rainbow angle (see, for example, Ref. 16), but we found it possible to recover the value of $\delta_\ell$ from the $\Theta(\ell)$ dependence. Namely, in the semi-classical treatments of scattering it is assumed that deflection is determined by the total phase shift (see the Appendix):

$$\Theta(\ell) = \frac{d(\delta_\ell + \delta_j(\ell))}{d\ell}. \quad (16)$$

If the $\Theta(\ell)$ and $\delta_j(\ell)$ dependencies are both known, this expression can be used as a differential equation for $\delta_\ell(\ell)$ with boundary condition $\delta_\ell(\infty) = 0$, which corresponds to no scattering at large impact parameters. Solving this equation numerically allows reconstructing the $\delta_\ell(\ell)$ dependence and expressing transition probability in Eq. (13) for the elastic channel as: $|\delta_{jj'}\delta_{ll'}\delta_{mm'} - S^J_{jj',ll',mm'}|^2 = |1 - a_{jm}\exp(i\delta_\ell)|^2$. Finally, this probability is averaged over $N$ trajectories using the Monte-Carlo method, just like in Eq. (15):

$$\sigma_{jm\to jm} = \frac{\pi}{k^2}\frac{J_{\max}}{N}\sum_i (2J^{(i)}+1)\left|1 - a^{(i)}_{jm}\exp(i\delta_\ell)\right|^2, \quad (17)$$

where the phase shift is computed from

$$\delta_\ell = -\int_\infty^\ell \Theta(s)ds - \delta_j(\ell), \quad (18)$$

where $s$ is a dummy variable introduced for integration over $\ell$.

### F. Differential cross sections

For simplicity of presentation, we will focus on differential cross section for the elastic channel ($j \to j$), but the procedure and conclusions are general and applicable to inelastic scattering as well. Scattering amplitude,

$$f_{jm\to jm}(\theta) = \frac{i}{k}\sum_{l=0}^{\infty}(2l+1)\left(1 - S^J_{jj,ll,mm}\right)P_l(\cos\theta), \quad (19)$$

is used to compute the differential cross section (averaged over the initial states $m$):

$$\frac{d\sigma_{j\to j}(\theta)}{d\Omega} = \frac{1}{(2j+1)}\sum_{m'=-j}^{j}\sum_{m=-j}^{j}\left|f_{jm\to jm'}(\theta)\right|^2. \quad (20)$$

In MQCT, the sum of Eq. (19) is replaced by a semi-classical integral over continuous distribution of $\ell$, and the phase $\delta_\ell$ is introduced (as above), which leads to

$$f_{jm\to jm}(\theta) = \frac{i}{k}\int_0^\infty (2\ell+1)(1 - a_{jm}\exp(i\delta_\ell))P_l(\cos\theta)d\ell. \quad (21)$$

Using Monte-Carlo approach this integral is computed as

$$f_{jm\to jm}(\theta) = \frac{i}{k_j}\frac{J_{\max}}{N}\sum_i (2\ell+1)\left(1 - a^{(i)}_{jm}\exp(i\delta_\ell)\right)P_l(\cos\theta). \quad (22)$$

### G. Numerical approach

As in full-quantum calculations, we used the potential energy surface expanded in terms of Legendre polynomials: $V(R, r, \gamma) = \sum V_k(R, r)P_k(\cos\gamma)$. For Na + $N_2(v = 0)$ system we included all even terms up to $k = 8$ and used the $R$-dependent expansion coefficients $V_k$ from Ref. 10. For He + $H_2$ system we included terms up to $k = 8$. Equations (1)–(7) were solved numerically altogether using Runge-Kutta method of 4th order. The initial molecule-quencher separation was close to $R = 28.2a_0$ in the case of Na + $N_2$ system and about $R = 24a_0$ in the case of He + $H_2$. Classical impact parameter, determined by convergence studies, was $b_{\max} = 24\,a_0$ in the case of Na + $N_2$ and $b_{\max} = 15\,a_0$ in the case of He + $H_2$. The magnitude of classical momentum is chosen as prescribed by the symmetrized average-velocity approach,[4] which takes into account microscopic reversibility of state-to-state transitions. In calculations with small $j$ the rotational basis set included all eigenstates up to $j = 14$ in the case of Na + $N_2$ system and up to $j = 12$ in the case of He + $H_2$. In one

case, quenching of $j = 22$ in He + $H_2$, we included all rotational states up to $j = 32$ and two vibrational states $v = 0$ and $v = 1$.

An important practical aspect is how to generate $P_l(\cos\theta)$ when $\ell$ is a continuous variable. In principle, one should replace a set of Legendre polynomials by their continuous analogue – the hyper-geometric function.[17] A FORTRAN routine from the package POLPAK for computation of the hyper-geometric functions worked fine for $\ell < 25$ but crashed at larger values of $\ell$. We also tried to compute hyper-geometric function using MATLAB, but at large $\ell$ this was inconveniently slow. As an alternative, we tried to round the value of $\ell$ to the closest integer and use polynomials, since they are fast to compute at any values of $\ell$. For the moderate values of $\ell$ the difference between the two methods was small and we finally adopted this approach.

In general, using a standard expansion of the PES in Jacobi coordinates $V(R, r, \gamma) = \sum V_k(R, r)P_k(\cos\gamma)$, one can evaluate matrix elements $M^{n'j'}_{nj}(R)$ as follows:

$$M^{n'j'}_{nj}(R) = \langle\phi_{nj}(r)\,|V_k(R,r)|\,\phi_{n'j'}(r)\rangle \begin{pmatrix} j' & k & j \\ -m & 0 & m \end{pmatrix} \times \begin{pmatrix} j' & k & j \\ 0 & 0 & 0 \end{pmatrix} \sqrt{(2j'+1)(2j+1)}(-1)^m. \quad (23)$$

A FORTRAN routine W3JS[18] was used to compute Wigner 3$j$ symbols. Note that matrix elements $\langle\phi_{nj}(r)\,|V_k(R,r)|\,\phi_{n'j'}(r)\rangle$ do not depend on $m$. Their values were computed on a grid of 400 points for along $2.0 < R < 25.0a_0$. In order to calculate derivatives in Eq. (4) a cubic spline was prepared for each such matrix element. Vibrational wave functions $\phi_{nj}(r)$ were calculated as prescribed in Ref. 4 using package ARPACK on an optimized grid of 128 points along $0.2 < r < 5.0a_0$.

## III. NUMERICAL RESULTS

### A. Tests of fully coupled MQCT method

Inelastic scattering calculations for Na + $N_2$ system were carried out in order to test accuracy of MQCT method in the case of reasonably heavy atomic masses. Full quantum CC results for this system are available from Ref. 11. Figure 2(a) summarizes data for excitation of the ground rotational state $j = 0$. Excitation cross sections were computed in a broad range of collision energies, $10 \le E \le 1100\,\text{cm}^{-1}$. Recall that for homo-nuclear $N_2$ in the initial state $j = 0$ the allowed transitions are: $0 \to 2$, $0 \to 4$, $0 \to 6$, *etc*. Analysis of Fig. 2(a) indicates that all these excitation processes are accurately reproduced by MQCT in a broad range of collision energies, and through four-orders-of-magnitude range of cross section values. Interestingly, as energy $E$ increases, the value of cross section for $0 \to 2$ slightly decreases, while it increases slightly for $0 \to 4$, and it passes through a pronounced maximum in the case of $0 \to 6$ transition. All these major features are reproduced well by MQCT (see Fig. 2(a)). But even less significant features, such as slight ondulations of the $\sigma(E)$ dependencies, are also reproduced by MQCT. Importantly, even the channel thresholds are correctly predicted.

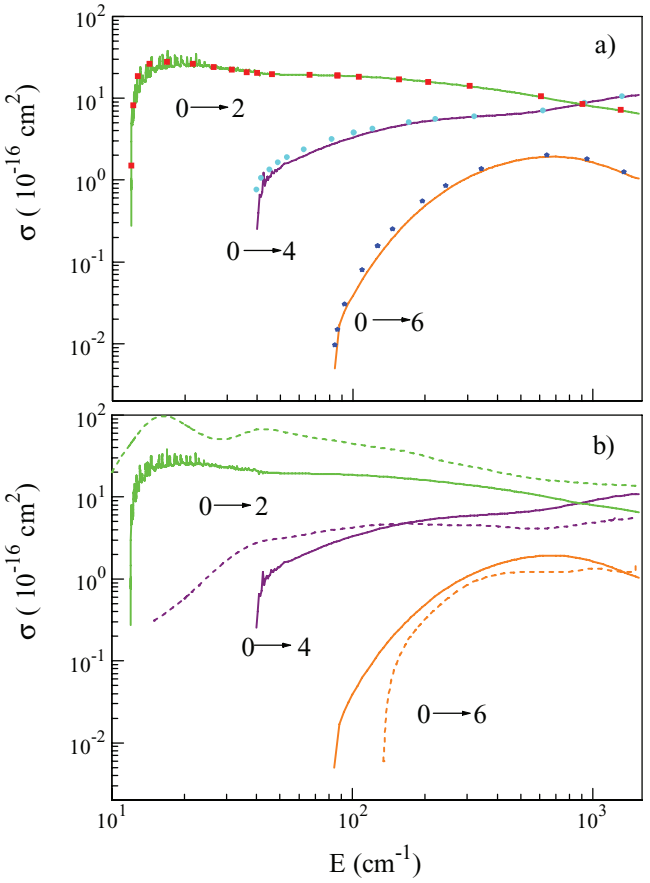


FIG. 2. Energy dependence of excitation cross sections for Na + $N_2$ system in the ground rotational state $j = 0$. Three allowed rotationally inelastic channels are shown for transitions into the excited states $j = 2$, $j = 4$, and $j = 6$. MQCT results are shown by symbols in frame (a), while classical trajectory results are shown by dashed lines in frame (b). Full-quantum data from Ref. 11 are shown by solid lines in both frames for comparison.

In Fig. 3(a) we summarized results for the inelastic transition processes that originate in the excited rotational state $j = 5$, located at energy $E = 59.7\,\text{cm}^{-1}$ above the ground rotational state. In this case the allowed excitation processes are: $5 \to 7$, $5 \to 9$, *etc.*, while the allowed quenching processes are $5 \to 3$ and $5 \to 1$. In all these cases MQCT reproduced quantum results very accurately in a broad range of collision energies and through five-orders-of-magnitude range of cross section values. Again, even small oscillations of $\sigma(E)$ dependencies for the processes $5 \to 3$ and $5 \to 1$ are correctly reproduced.

Inelastic scattering calculations for He + $H_2$ system were carried out in order to test accuracy of MQCT method in the limit of lightest atomic masses. This example is often thought of as an essentially non-classical system, the worst-case scenario for, and the stringent possible test of, the mixed quantum/classical method. Full quantum benchmark data for this system are available from Refs. 12 and 13. Figure 4 summarizes results for quenching or two lowest excited rotational states, the processes $2 \to 0$ and $4 \to 2$, at collision energies in the range $1 \le E \le 10\,000\,\text{cm}^{-1}$. We see that, indeed, in this light system the deviations of MQCT from quantum benchmark are more noticeable, and occur in a somewhat larger range of collision energies, compared to more classical Na

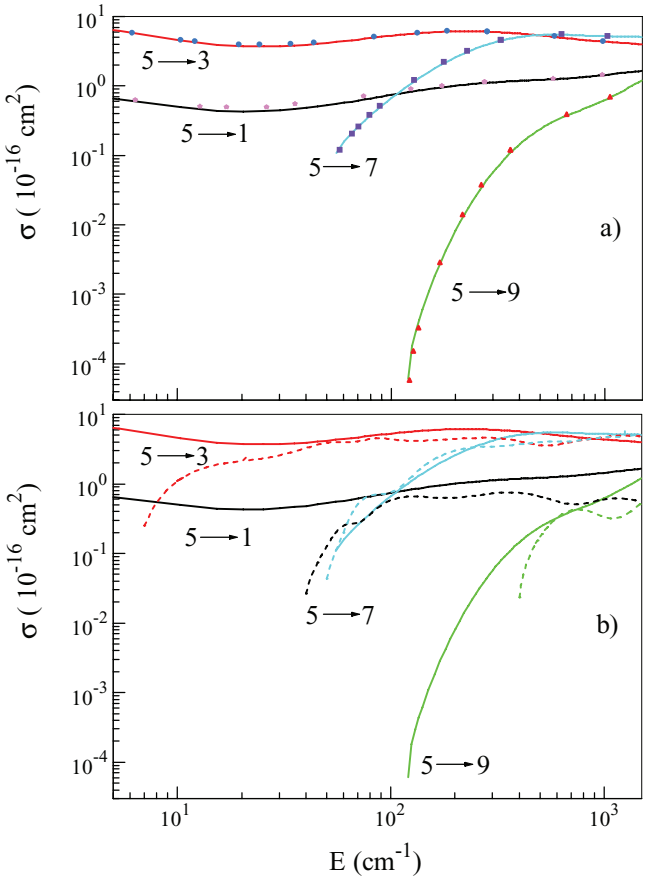


FIG. 3. Energy dependence of inelastic cross sections for Na + $N_2$ system in the excited rotational state $j = 5$. Two excitation channels correspond to allowed transitions into $j = 7$ and $j = 9$. Two quenching channels correspond to allowed transitions into $j = 1$ and $j = 3$. MQCT results are shown by symbols in frame (a), while classical trajectory results are shown by dashed lines in frame (b). Full-quantum data from Ref. 11 are shown by solid lines in both frames for comparison.

+ $N_2$ system. However, the values of these deviations are still relatively small. For example, at $E = 25\,\text{cm}^{-1}$ the deviations are only 15% and 25% for processes $2 \rightarrow 0$ and $4 \rightarrow 2$, respectively. Interestingly, at even lower collision energies, the accuracy of MQCT remains about the same, it does not worsen significantly even at $E = 2\,\text{cm}^{-1}$. But, as energy increases, MQCT results merge monotonically with full quantum results. For $2 \rightarrow 0$ excellent agreement is found above $E = 100\,\text{cm}^{-1}$. For $4 \rightarrow 2$ the agreement improves significantly when collision energy approaches $E = 200\,\text{cm}^{-1}$. Note that the dependence of cross section in Fig. 4 goes through minimum and maximum and those features are reproduced well by MQCT. Thus, MQCT is applicable even to this light and highly non-classical system, and it remains reasonably accurate even at low collision energies.

### B. Test of CS-approximation

Figure 5 shows the same data as in Fig. 2(a), but obtained using the approximate CS-version of MQCT, derived in Sec. II C. Overall, the quality of these data is very reasonable. Deviations from the full quantum benchmark are observed for all three processes: $0 \rightarrow 2$, $0 \rightarrow 4$, and $0 \rightarrow 6$, but typically they

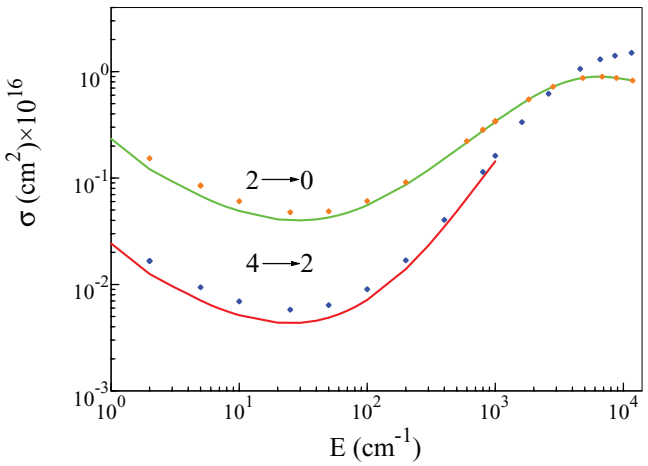


FIG. 4. Energy dependence of quenching cross sections for He + $H_2$ system. Two transitions are shown, one from $j = 4$ into $j = 2$, and the other from $j = 2$ into $j = 0$. MQCT results are shown by symbols. Full-quantum data from Ref. 12, where available, are shown by solid lines for comparison.

do not exceed 25% (somewhat more near the channel threshold). Overall, one should admit that the fully coupled version of MQCT is in much better and more detailed agreement with exact quantum results (compare Fig. 5 *vs.* Fig. 2(a)).

For Na + $N_2$ system the CS-version of theory was faster, but not by much, just by a factor of ×3. For more complicated systems (triatomic + atom or triatomic + diatomic) the computational speed up may be more substantial, but one should keep in mind that accuracy of CS approximation is non-uniform. For example, we found that for $0 \rightarrow 2$ transition at lower collision energies the value of CS cross section is larger, while at higher collision energies it is smaller, compared to the fully coupled MQCT data and quantum benchmark data. The switching occurs near $E = 50\,\text{cm}^{-1}$, which produces an artificial oscillation of the CS cross section, quite different from the benchmark data. In contract, the fully coupled version of MQCT gives detailed and uniformly reliable description through the entire range of collision energies.

Full quantum calculations are very demanding at high collision energies and for highly excited rotational states.

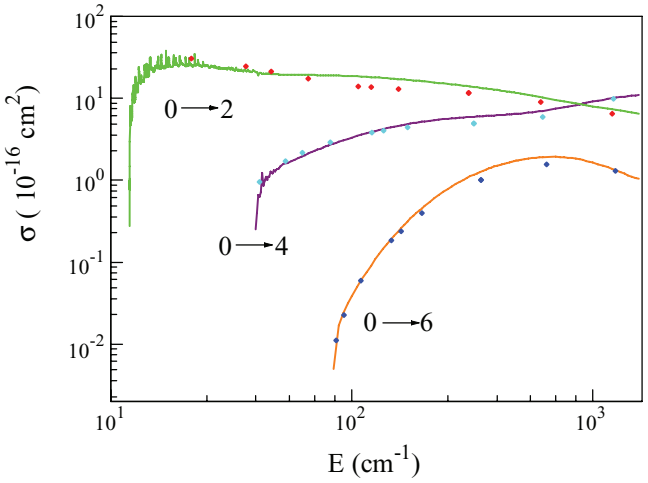


FIG. 5. Same as in Fig. 2(a), but using an approximate CS-version of MQCT.

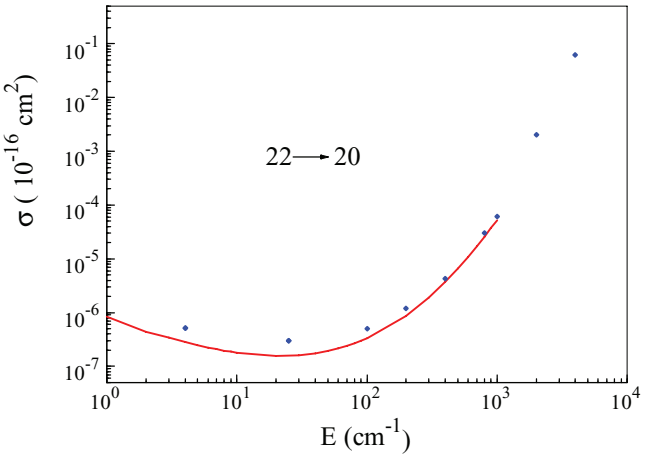


FIG. 6. Energy dependence of cross section for quenching of $j = 22$ into $j = 20$ in He + $H_2$ system. CS-version of MQCT is used (symbols) and compared to full-quantum CS method (solid line) from Ref. 13, where available.

At such conditions the exact CC-method is almost never used, and the CS-approximation is usually adopted. For He + $H_2$ system at high levels of rotational excitations such (full quantum but approximate) CS results are available from literature[12,13] and web site of one of the authors.[19] We carried out similar calculations using MQCT. Figure 6 presents our MQCT-SC results for rotational quenching of $j = 22$ in comparison with quantum benchmark data. The dominant process is 22 → 20, and the corresponding transition energy is huge, $\Delta E = 2,967.6\,\text{cm}^{-1}$. Results of MQCT are accurate at collision energies above $350\,\text{cm}^{-1}$. For this transition, no quantum CS results are available above $E = 1000\,\text{cm}^{-1}$, but we easily computed few points up to $E = 10\,000\,\text{cm}^{-1}$. Moreover, it should be noted that in the He + $H_2$ system in $j = 22$ and at this collision energy the *vibrational* state-to-state transitions become important and should also be included, in addition to rotational state-to-state transitions. The calculations we did were such ro-vibrational calculations. However, in present paper we prefer to restrict discussion to *rotational* transitions only.

### C. Criterion of accuracy

According to Delos criterion for atom-atom collisions,[14] and by analogy with our earlier findings from MQCT calculations of *vibrational* quenching,[5] the MQCT method is expected to be more accurate when the energy change $\Delta E$ associated with quantum state-to-state transition is small. Similar conclusion can be deduced from our data for Na + $N_2$ system presented in Fig. 2(a). For example, the transition 0 → 2, which has smallest value of $\Delta E = 11.9\,\text{cm}^{-1}$, is reproduced by MQCT particularly well. For this process the deviation from full quantum result is observed only near the channel threshold, and this discrepancy vanishes quickly as collision energy is increased. If we look at transitions 0 → 4 and 0 → 6, where the values of energy quantum rise to $\Delta E = 39.8\,\text{cm}^{-1}$ and $83.5\,\text{cm}^{-1}$, respectively, we start seeing some deviations from full quantum results slightly further from the channel threshold. This behavior is understood and even expected near the channel threshold, where $E \approx \Delta E$. Roughly, results of Fig. 2(a) show that MQCT becomes very accurate at collision energies $E > 2\Delta E$. But even in the energy range $\Delta E < E < 2\Delta E$ the results of MQCT are quite reasonable.

Most interestingly, we found that MQCT is particularly accurate for the rotationally excited states. This makes sense, since excited states are more classical. For example, the four sets of data presented in Fig. 3(a) still correspond to relatively large values of $\Delta E$: $35.8\,\text{cm}^{-1}$, $51.7\,\text{cm}^{-1}$, $55.7\,\text{cm}^{-1}$, and $119.4\,\text{cm}^{-1}$. Nevertheless, the excitation cross sections computed by MQCT for 5 → 7 and 5 → 9 are very accurate (even at the channel threshold, $E = \Delta E$), and the quenching cross for 5 → 3 and 5 → 1 are accurate at *any* energies we considered, down to $E = 5\,\text{cm}^{-1}$ (because there is no threshold for quenching). No any obvious criterion can be formulated or needed here. MQCT data are simply almost as accurate as the full quantum data.

In the case of He + $H_2$ system the state-to-state transition energies $\Delta E$ are large: $384\,\text{cm}^{-1}$ and $813\,\text{cm}^{-1}$ for the processes 2 → 0 and 4 → 2, respectively. From one side, this explains why deviations of MQCT results from quantum benchmark are larger in this system than in Na + $N_2$. But from another side, this also means that the criterion for validity of MQCT may be less stringent. Namely, for He + $H_2$, MQCT is rather accurate at collision energies above $E = 100\,\text{cm}^{-1}$ for transition 2 → 0, and above $E = 200\,\text{cm}^{-1}$ for transition 4 → 2. Roughly, this corresponds to $E > \Delta E/4$. And again, this is for the lower, most quantum mechanical states. Excited rotational states are more classical. For transition 22 → 20 we have $\Delta E = 2967.6\,\text{cm}^{-1}$and MQCT is accurate above $350\,\text{cm}^{-1}$ which, in fact, is much better than $\Delta E/4$ (this is closer to $\Delta E/8$). This example gives clear indications where the range of applicability and the predictive power of MQCT approach are.

For all integral cross sections discussed above and both benchmark systems studied here we computed relative errors of MQCT method (% of the full-quantum result) and collected them all together in Fig. 7. Only a few outlying points were not included into this graph. Both excitation and quenching processes were included. Horizontal axis gives the ratio $\Delta E/E$, and the range of its values is rather large, $10^{-2} < \Delta E/E < 10^3$. More accurate corner of this graph corresponds to low $\Delta E$ and high $E$, while less accurate corner corresponds to high $\Delta E$ and low $E$. Despite some spread of points present in these data, the plot in Fig. 7 shows clear correlation between accuracy and the value of $\Delta E/E$. We found that the data for He + $H_2$ and for Na + $H_2$ complement each other, following very similar trends. Thus, we conclude that this dependence is rather general and we recommend using this picture to estimate the error of MQCT method before applying it to new systems. For example, consider rotational quenching from the first excited rotational state to the ground state in $H_2O$, $NH_3$ and in $HCOOCH_3$ (methyl formate, small organic molecule important for astrophysics). Rotational quanta in these molecules are $\Delta E = 18.6\ \text{cm}^{-1}$, $16.3\ \text{cm}^{-1}$, and $0.41\ \text{cm}^{-1}$, respectively. Neither of these systems was studied using MQCT, but we plan doing such calculations in the future. From Fig. 7 one can expect that at energy of collision $E = 100\,\text{cm}^{-1}$an error of MQCT should be no more than 2%

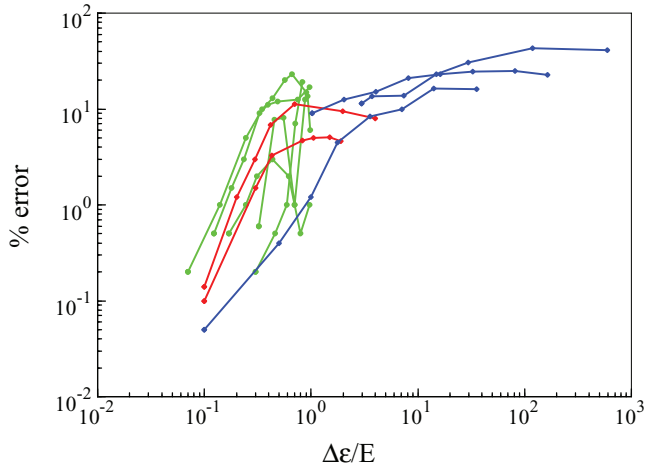


FIG. 7. Percent error of MQCT method for all calculations of this paper. The value of error correlates with the ratio of transition energy to scattering energy. Quenching processes for Na + $N_2$ are plotted using red solid lines, while excitation processes are plotted using green lines. The data for He + $H_2$ are blue.

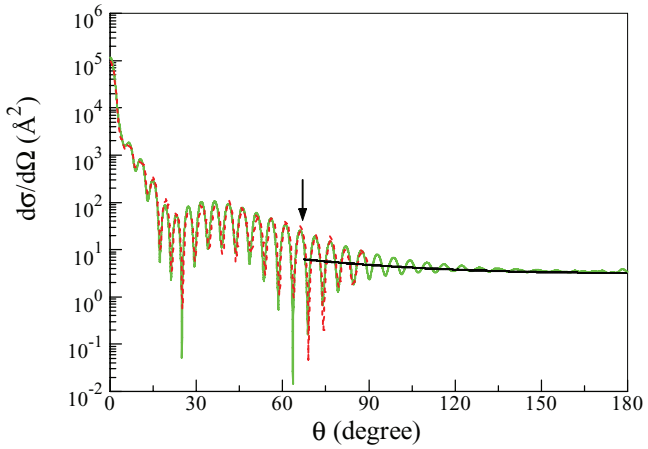


FIG. 8. Differential cross section for the elastic scattering channel of Na + $N_2(j = 0)$ system at collision energy $E = 50\,\mathrm{cm}^{-1}$. MQCT results are shown by red dashed line. Full-quantum data from Ref. 11 are shown by green solid line for comparison. Classical rainbow angle is indicated by arrow. A pseudo-classical (see text) cross section is shown by black solid line in the range of angles beyond the rainbow.

for $H_2O$ and $NH_3$, and no more than 0.5% for methyl formate. At higher collision energies the errors are expected to be smaller. When MQCT results for these new molecules become available, they can be added to this graph, in order to improve predictive capability of the method.

One can also notice that the full quantum data for Na + $N_2$ system (from Ref. 11, used here as a benchmark) exhibit some resonances just above threshold, especially in the case of $0 \rightarrow 2$ transition shown in Fig. 2(a). It is an interesting general question whether MQCT can be used to treat these purely quantum features of cross section. For example, classical trajectory capture is analog of quantum scattering resonance, and we saw that at energies close to threshold many trajectories were captured in the interaction region. Analysis of these trajectories may give some useful information about scattering resonances, but we decided to postpone exploration of this topic to future work, and do that for a different system, with fewer isolated resonances. Here, we restricted our analysis to non-resonant cross sections only and simply zeroed all trajectories that exhibited resonant behavior.

### D. Differential cross sections

Figure 7 presents differential cross section for the elastic scattering channel of Na + $N_2$ ($j = 0$) system at relatively low collision energy $E = 50\,\mathrm{cm}^{-1}$. Figures 8(a) and 8(b) show the same for higher collision energies, $E = 100\,\mathrm{cm}^{-1}$ and $E = 700\,\mathrm{cm}^{-1}$, respectively. In all these cases the full quantum benchmark data are available from Ref. 11. We see that dependence of cross section on scattering angle is highly oscillatory (non-classical) but MQCT method reproduces every single oscillation of this dependence very accurately. To our best knowledge this is the first application of mixed quantum/classical theory to calculation of differential scattering cross section.

Recall that classical scattering theory works only at large scattering angles, beyond the classical rainbow angle (small impact parameters, backscattering). At the rainbow angle the classical scattering cross section diverges (see the Appendix), and it is poorly defined at angles smaller than the rainbow angle (large impact parameters). Various versions of semi-classical treatment of scattering exist, capable of removing singularity at the rainbow angle,[18] and expanding the range of validity of the classical scattering theory slightly into the quantum scattering regime (vicinity of the rainbow angle). No semi-classical treatment of scattering is expected to work at small scattering angles, in the quantum scattering regime.

It is encouraging that MQCT is very accurate at small scattering angles, in the quantum scattering regime. Note that in Fig. 8 logarithmic scale is applied to the horizontal axis, in order to emphasize the small scattering angle part of cross section dependence. The rainbow angle is also marked in Figs. 7 and 8, and we see that in its vicinity the dependence of MQCT cross section is regular, just as quantum benchmark data, and is very accurate.

Unexpectedly, we found that differential cross sections computed by MQCT exhibit unphysical behavior at *large* scattering angles (not shown here), in the classical scattering regime, where even a simple classical mechanics is expected to work! This behavior is not yet completely understood, and most probably is due to some technical issue, but we found a temporary fix for it. In Figs. 7 and 8 we also plotted a pseudo-classical cross section, obtained simply by differentiating the classical deflection function $\Theta(\ell)$ derived from MQCT calculations (see Eq. (A15) in the Appendix). At scattering angles larger than rainbow angle such cross section is well defined and comparison with full quantum data shows that it sets up accurately the asymptotic trend (see Figs. 7 and 8). Thus, at large scattering angles one can easily switch to this pseudo-classical cross section.

Finally, the integral elastic scattering cross section, obtained by integrating the differential cross sections discussed above, is presented in Fig. 9. The agreement with quantum benchmark data is rather good, down to collision energies $E$

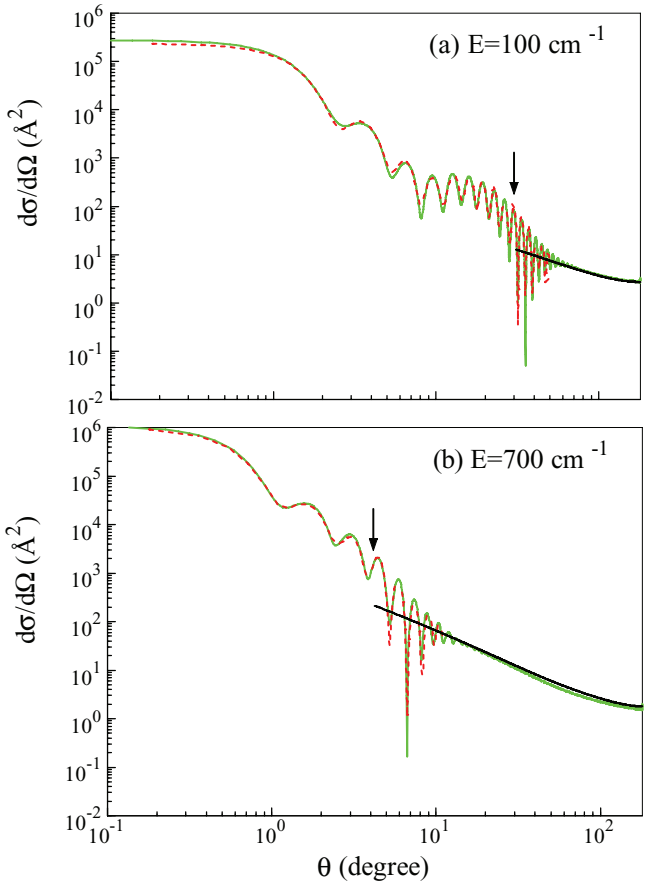


FIG. 9. Differential cross section for the elastic scattering channel of Na + $N_2$($j = 0$) system at collision energies $E = 100\,\mathrm{cm}^{-1}$ and $700\,\mathrm{cm}^{-1}$ in frames (a) and (b), respectively. MQCT results are shown by red dashed line. Full-quantum data from Ref. 11 are shown by green solid line for comparison. Classical rainbow angle is indicated by arrow. A pseudo-classical (see text) cross section is shown by black solid line in the range of angles beyond the rainbow. This figure emphasizes small scattering angles (note logarithmic scale in the horizontal axis).

$= 50\,\mathrm{cm}^{-1}$ or so. At even lower energies we start seeing deviations, but the overall trend of dependence is captured well by MQCT: it goes through maxima and minima several times and these quantum oscillations are all reproduced (see Fig. 10). Recall that classical scattering theory cannot predict the elastic scattering cross section, because the maximum impact parameter is impossible to define rigorously. In contrast, MQCT uses phase information (just as full quantum method) which avoids the problem. In the range of collision energies where MQCT is accurate it can be used to predict the elastic scattering cross sections reliably.

As discussed in the theory section above, calculations of differential cross sections and elastic scattering cross sections use phase information and quantum interference. These phenomena are very sensitive to errors and when MQCT becomes less accurate overall (at lower scattering energies) these cross sections suffer the most. For example, we also calculated the differential cross section at low collision energy $E = 15\,\mathrm{cm}^{-1}$ (in the region of scattering resonances), but in this case we found larger discrepancies between MQCT results and the full quantum benchmark data. So, at very low collision energies one should be careful using MQCT to predict differential cross sections or the elastic scattering cross sections.

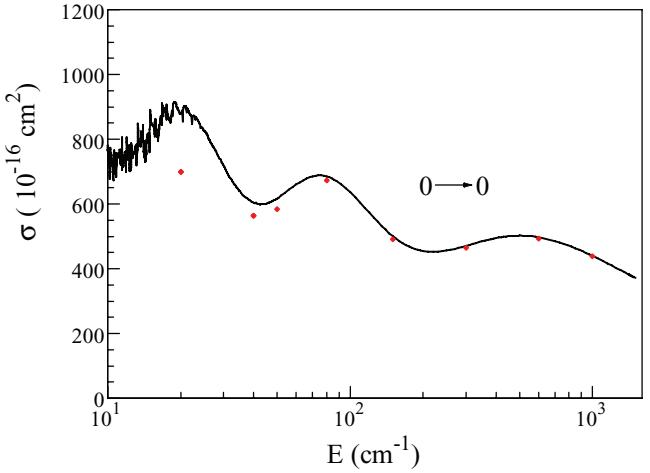


FIG. 10. Energy dependence of integral cross section for the elastic scattering channel of Na + $N_2$ system in the ground rotational state $j = 0$. MQCT results are shown by symbols. Full-quantum data from Ref. 11 are shown by solid line for comparison.

### E. Purely classical trajectories

In MQCT formalism of rotational quenching the classical mechanics is used only for description of scattering, while quantum mechanics is used for rotational state-to-state transitions. Why not to get rid of the quantum mechanics entirely, and treat all degrees of freedom classically? This was attempted in the past and, in particular, it was shown that for the He + $H_2$ system at collision energies close to $E = 1000\,\mathrm{cm}^{-1}$ the value of cross section for transition $2 \rightarrow 0$ is underestimated by an order of magnitude or so.[12] At collision energies lower than $E = 1000\,\mathrm{cm}^{-1}$ it is expected to be even worse. Performance of the classical trajectory method for He + $H_2$ system improves only when the collision energy reaches $E = 4000\,\mathrm{cm}^{-1}$ or so, but the agreement with full quantum method still remains rather rough.[12]

For heavy atoms classical mechanics is expected to work somewhat better, and we decided to run the purely classical trajectory simulations for Na + $N_2$ system. We tried several known methods of the final state analysis but we found that, when applied to various needed state-to-state cross sections in a broad range of energies, neither method works consistently better than others (although, we did not attempt the Gaussian binning[20]). Results presented below were obtained using the prescription of Bowman,[21] which worked slightly better. Furthermore, since $N_2$ is symmetric, we had to introduce an *ad hoc* factor of $\times 1/2$ (which would be hard to justify in the case of different isotopes). Only then the results of classical trajectory simulations for Na + $N_2$ fall into the right order of magnitude range (Fig. 10).

Our classical results are summarized in Figs. 2(b) and 3(b). They can be conveniently compared to the full quantum benchmark data and to our MQCT results as well, shown in Figs. 2(a) and 3(a). We see that although not all, but many $\sigma(E)$ dependencies are similar. However, the quality of

agreement is qualitative (at best), rather than quantitative. Some of the classical state-to-state cross sections are higher while others are lower compared to quantum results. Large deviations by a factor of 2–4 are typical. Moreover, near the channel thresholds (for excitation processes) and at lower collision energy (for quenching processes) the deviations are particularly large and often reach two orders of magnitude. In terms of accuracy for rotational state-to-state transition cross sections, the classical trajectory method is not even close to MQCT.

Finally, we found that, from the computational standpoint, the classical trajectory simulations are even *more* demanding than MQCT. This seems surprising first, but has simple explanation. It appears that at low collision energy, when the value of transition cross section is small (and many cross sections in Figs. 2(a) and 3(a) are very small) one needs to sample literally hundreds of thousands of classical trajectories, in order to find that rare event (special collision arrangement) that makes non-zero contribution to cross section. In addition to everything said above, the classical cross sections at low energies are typically poorly converged and very expensive computationally. MQCT is the method of choice. It is almost as accurate as the full quantum method, and is computationally cheaper than the classical trajectory method.

## IV. CONCLUSIONS

In this paper we carried out the first extensive benchmarking of accuracy of the MQCT treatment of rotationaly inelastic scattering processes. Two molecular systems were considered, one of which contained all light atoms ($He + H_2$), while the other one contained all reasonably heavy atoms ($Na + N_2$). A broad range of classical collision energies was explored: $1 < E < 10\,000\,cm^{-1}$. The values of quantum state-to-state transition energies studied here also covered a wide range: $10 < \Delta E < 3000\,cm^{-1}$. The amount of initial rotational excitation varied from $j = 0$ to $j = 22$. The values of obtained scattering cross sections varied from $10^{-23}$ to $10^{-13}\,cm^2$. In addition to energy dependence of integral cross sections, we also looked at the differential (over scattering angle) cross sections. Both elastic and inelastic scattering channels were studied. In all these cases a detailed comparison of MQCT against the full quantum method was carried out.

We found that in many of these cases the results of MQCT are hard to distinguish from the full quantum (CC) results. We also saw that in some unfavorable cases (low mass, low collision energy, and large transition energy) MQCT becomes less accurate, but we never really saw it failing. For example, in the worst-case situations the values of MQCT cross sections were overestimated by 25% or so, which still can be characterized as a semi-quantitative agreement. And this is in the lightest possible system, $He + H_2$. In all other chemically relevant molecular systems, at thermal collision energies, MQCT is expected to be much more accurate than this.

As a rule of thumb, one can probably use the following criterion for rotational quenching processes: *When* $E > \Delta E/4$ *the results of MQCT become accurate to within few percent, compared to full quantum data.* Most importantly is that MQCT results approach the full quantum results monotonically, in a predictable way. Above $E = \Delta E/4$ they are very accurate, below $E = \Delta E/4$ they start deviating from the full quantum data, but this deviation does not increase rapidly. We saw that MQCT always produces reasonable data, even in unfavorable situations, when it is less accurate.

It seems that this method represents a useful alternative to the full quantum methods in situations when collisional energies are high, rotational excitation is significant, masses are large and the densities of states are large (small state-to-state transition energies). These cases are hard to handle numerically using the full quantum methods, such as CC, but MQCT becomes very accurate in these same situations. Of course, larger number of states involved in expansion of wave function will make any calculations more demanding, both CC and MQCT, but overall the mixed quantum/classical approach is much more affordable.

The computational cost of MQCT is really low. For small values of $j$ in both systems considered here, only about 1 min on single processor was spent per energy point. It is still hard to say how this will grow with size of the molecule, since we only start applying this theory to triatomic + atom systems. However, we want to stress that MQCT calculations for different trajectories are entirely independent (sampling over $\ell$), which makes this method intrinsically and embarrassingly parallel. One can easily spread MQCT trajectories onto hundreds of processors with zero communication overlap. With this capability, MQCT calculations are expected to be affordable even for polyatomic molecules, with large number of states included, and even without the CS-approximation involved. It is also important to note that propagation of MWCT trajectories is computationally faster at higher collision energies, which makes this method appealing for high temperature applications.

One more appealing aspect of MQCT methodology is that it offers a unique time-dependent insight into mechanism of the process. Indeed, although the standard time-independent scattering theory provides the transition matrix and characterizes completely the outcome of molecular collision, it tells us nothing about the course of the process, how wave function of the system evolves in time and space. In our MQCT approach and other related time-dependent methods[22,23] one can monitor how state populations $|a_{j'm'}|^2$ change as collision progresses along the trajectory. Do the populations change monotonically and describe direct transitions, or there is a temporary population transfer to some intermediate states? And what is the time scale of the process? These opportunities will be explored in the near future.

## ACKNOWLEDGMENTS

R. Forrey (Penn State, Berks), N. Balakrishnan (University of Nevada, Las Vegas), and P. Zhang (Harvard University) are gratefully acknowledged for sharing their data and potential energy surfaces. This research was supported by NSF, partially through the Atmospheric Chemistry Program, Grant No. 1252486, and partially through the Chemical Theory, Models and Computational Methods Program, Grant No. 1012075. This research used resources of the National Energy Research

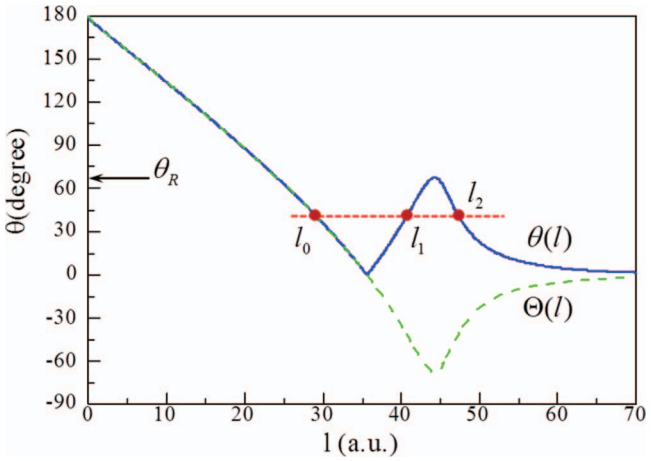


FIG. 11. Pseudo-classical deflection and scattering functions from MQCT calculations. Scattering function $\theta(\ell)$ is always positive (solid line), while deflection function $\Theta(\ell)$ is always smooth (dashed line). Classical rainbow angle is indicated. At angles below this value three branches of scattering function contribute and interfere (quantum scattering regime). At angles above this value only one branch contributes and scattering is classical.

Scientific Computing Center, which is supported by the Office of Science of the U.S. Department of Energy under Contract No. DE-AC02-05CH11231.

## APPENDIX: SEMI-CLASSICAL THEORY OF SCATTERING

Figure 11 represents example of classical scattering function $\theta(\ell)$ and deflection function $\Theta(\ell)$ obtained from MQCT calculations for Na + $N_2$ ($j = 0$) system at collision energy $E = 50\,\mathrm{cm}^{-1}$. The "rainbow" angle is observed at 67.5°. At scattering angles larger than rainbow angle only one branch of the $\Theta(\ell)$ dependence contributes to the differential cross section and the scattering is classical (small values of $\ell$, small impact parameters). At angles smaller than rainbow angle several branches contribute (three in Fig. 11), producing interference. So, small scattering angles correspond to quantum scattering regime (large values of $\ell$, large impact parameters).

When $(l + 1/2)\sin\theta \gg 1$ it is usual to approximate Legendre polynomials in Eq. (21) by the following expression:[16]

$$P_l(\cos\theta) \approx -\frac{i}{\sqrt{2\pi l \sin\theta}}\left[\exp\left\{i\left(\left(l+\frac{1}{2}\right)\theta+\frac{\pi}{4}\right)\right\} - \exp\left\{i\left(-\left(l+\frac{1}{2}\right)\theta-\frac{\pi}{4}\right)\right\}\right]. \quad \text{(A1)}$$

Also, as explained in Sec. II D, the elastic element of transition matrix is $1 - a(l)\exp\{i\delta_l\} = 1 - |a(l)|\exp\{i(\delta_j + \delta_l)\}$, where, in order to simplify notations, we omitted subscripts in $a(l)$. Using these expressions the integral of Eq. (21), we can split it onto three terms:

$$f(\theta) = \frac{1}{2k}\int_0^\infty \frac{(2l+1)\,|a(l)|}{\sqrt{2\pi\, l \sin\theta}} \times \exp\left\{i\left(\delta_l+\delta_j-\left(l+\frac{1}{2}\right)\theta-\frac{\pi}{4}\right)\right\} dl$$

$$-\frac{1}{2k}\int_0^\infty \frac{(2l+1)\,|a(l)|}{\sqrt{2\pi\, l \sin\theta}} \times \exp\left\{i\left(\delta_l+\delta_j+\left(l+\frac{1}{2}\right)\theta+\frac{\pi}{4}\right)\right\} dl$$

$$+\frac{1}{2ik}\int_0^\infty (2l+1)P_l(\cos\theta)dl. \quad \text{(A2)}$$

The last term is equal to zero and does not affect the differential cross section. The first two terms are estimated using the stationary phase approximation. Namely, the main contribution to the first integral is given by small $\ell$ (repulsive short range interaction) where the phase reaches a local maximum.[16] In other words

$$\frac{d}{dl}\left(\delta_l+\delta_j-\left(l+\frac{1}{2}\right)\theta-\frac{\pi}{4}\right)=0, \quad \text{(A3)}$$

which gives us the condition:

$$\frac{d(\delta_l+\delta_j)}{dl} = +\theta. \quad \text{(A4)}$$

Similar arguments for the second term in (A2) give us

$$\frac{d(\delta_l+\delta_j)}{dl} = -\theta. \quad \text{(A5)}$$

Combining these two expressions, we have

$$\frac{d(\delta_l+\delta_j)}{dl} = \pm\theta = \Theta(l). \quad \text{(A6)}$$

In semi-classical treatment $\Theta(l)$ is assumed to be the classical deflection function. This finalizes derivation of Eq. (16) used in Sec. II D.

Note that in our MQCT calculations of differential cross sections we neither use the approximation of Eq. (A1) for $P_l(\cos\theta)$ nor estimate $f(\theta)$ from Eq. (A2). Instead, we use Eq. (A6) only to recover the value of scattering phase $\delta_l$ (see Eq. (18)), and then we substitute $\delta_l$ into the exact Eq. (21), without any approximations. This must be the reason why MQCT treatment works well even at small scattering angles, where the usual semi-classical theory of scattering (outlined below) does not work.

In order to continue manipulations with Eq. (A2), for given $\theta$ we can find a stationary point $l_0$ (or, in the quantum regime, several such points: $l_0$, $l_1$, and $l_2$) and expand the argument in its vicinity using Taylor series to 2nd order. First derivative is equal to zero since $l_0$ is extremum. Second derivative:

$$\frac{\partial^2}{\partial l^2}\left(\delta_l+\delta_j-\left(l+\frac{1}{2}\right)\theta-\frac{\pi}{4}\right) = \frac{\partial^2}{\partial l^2}(\delta_l+\delta_j) = \frac{\partial\Theta(l)}{\partial l}, \quad \text{(A7)}$$

where we used Eq. (16). The expansion is

$$\delta_l+\delta_j-\left(l+\frac{1}{2}\right)\theta-\frac{\pi}{4} \approx \delta_l(l_0)+\delta_j(l_0)-\left(l_0+\frac{1}{2}\right)\theta - \frac{\pi}{4}+\frac{\partial\Theta(l_0)}{\partial l}\frac{(l-l_0)^2}{2} = -\int_\infty^{l_0}\Theta(s)ds-\left(l_0+\frac{1}{2}\right)\theta$$

$$-\frac{\pi}{4}+\frac{\partial\Theta(l_0)}{\partial l}\frac{(l-l_0)^2}{2}, \tag{A8}$$

where we used Eq. (18). Substitution of this argument into the first integral in Eq. (A2) gives

$$\frac{1}{k}\int_{-\infty}^{\infty}\frac{\left(l_0+\frac{1}{2}\right)|a(l_0)|}{\sqrt{2\pi\, l_0\sin\theta}}\exp\left\{i\left(-\int_{\infty}^{l_0}\Theta(s)ds-\left(l_0+\frac{1}{2}\right)\theta\right.\right.$$
$$\left.\left.-\frac{\pi}{4}+\frac{\partial\Theta(l_0)}{\partial l}\frac{(l-l_0)^2}{2}\right)\right\}dl=\frac{\left(l_0+\frac{1}{2}\right)|a(l_0)|}{k\sqrt{2\pi\, l_0\sin\theta}}$$
$$\times\exp\left\{i\left(-\int_{\infty}^{l_0}\Theta(s)ds-\left(l_0+\frac{1}{2}\right)\theta-\frac{\pi}{4}\right)\right\}\int_{-\infty}^{\infty}$$
$$\times\exp\left\{i\left(\frac{\partial\Theta(l_0)}{\partial l}\frac{(l-l_0)^2}{2}\right)\right\}dl. \tag{A9}$$

The last factor here can be computed using Fresnel's integral:

$$\int_{-\infty}^{\infty}\exp\left\{i\left(\frac{\partial\Theta(l_0)}{\partial l}\frac{(l-l_0)^2}{2}\right)\right\}dl=\sqrt{\frac{2\pi}{\frac{\partial\Theta(l_0)}{\partial l}}}\exp\left\{i\frac{\pi}{4}\right\}. \tag{A10}$$

Substitution of this result into Eq. (A9) leads to

$$\frac{\left(l_0+\frac{1}{2}\right)|a(l_0)|}{k\sqrt{2\pi l_0\sin\theta}}$$
$$\times\exp\left\{i\left(-\int_{\infty}^{l_0}\Theta(s)ds-\left(l_0+\frac{1}{2}\right)\theta-\frac{\pi}{4}\right)\right\}\sqrt{\frac{2\pi}{\frac{\partial\Theta(l_0)}{\partial l}}}\exp\left\{i\frac{\pi}{4}\right\}$$
$$=\frac{\left(l_0+\frac{1}{2}\right)|a(l_0)|}{k\sqrt{l_0\sin\theta\frac{\partial\Theta(l_0)}{\partial l}}}\exp\left\{i\left(-\int_{\infty}^{l_0}\Theta(s)ds-\left(l_0+\frac{1}{2}\right)\theta\right)\right\}$$
$$=\frac{\left(\sqrt{l_0}+\frac{1}{2\sqrt{l_0}}\right)|a(l_0)|}{k\sqrt{\sin\theta\frac{\partial\Theta(l_0)}{\partial l}}}\exp\left\{i\left(-\int_{\infty}^{l_0}\Theta(s)ds-\left(l_0+\frac{1}{2}\right)\theta\right)\right\}$$
$$\approx\frac{\sqrt{l_0}\,|a(l_0)|}{k\sqrt{\sin\theta\frac{\partial\Theta(l_0)}{\partial l}}}\exp\left\{i\left(-\int_{\infty}^{l_0}\Theta(s)ds-\left(l_0+\frac{1}{2}\right)\theta\right)\right\}. \tag{A11}$$

Here we assumed that $l_0\gg1$. This is the final result for the first integral in Eq. (A2).

Similar considerations are applicable to the second integral in Eq. (A2), but in the classical scattering regime (single branch of the deflection function, single extremum $l_0$) the second integral is always oscillatory and makes no contribution to $f(\theta)$. However, in the quantum scattering regime, each additional branch of the deflection function produces one additional extremum ($l_1$ and $l_2$ in Fig. 11). At such conditions the second integral in Eq. (A2) gives

$$\frac{\sqrt{l_1}\,|a(l_1)|}{k\sqrt{\sin\theta\left|\frac{\partial\Theta(l_1)}{\partial l}\right|}}\exp\left\{i\left(-\int_{\infty}^{l_1}\Theta(s)ds+\left(l_1+\frac{1}{2}\right)\theta\right)\right\}, \tag{A12}$$

for $l_1$, and similar for $l_2$. Combining all branches of the deflection function and using $\pm\theta=\Theta$, we finally obtain a semi-classical expression for scattering amplitude:

$$f(\theta)=\sum_q\frac{\sqrt{l_q}\,|a(l_q)|}{k\sqrt{\sin\theta\left|\frac{\partial\Theta(l_q)}{\partial l}\right|}}$$
$$\times\exp\left\{i\left(-\int_{\infty}^{l_q}\Theta(s)ds-\left(l_q+\frac{1}{2}\right)\Theta(l_q)\right)\right\}, \tag{A13}$$

where the sum is over $q$ branches of the deflection function $\Theta(l)$ (e.g., three in Fig. 11).

We tried this semi-classical method for differential cross section and found that indeed the Eq. (A13) allows removing singularity at the rainbow point and gives correct asymptotic value of cross section at large scattering angles (as $\theta\to\pi$, backscattering, classical regime). However, it fails to reproduce quantum oscillations of cross section seen in Figs. 7 and 8. Also, it is rather inaccurate at small scattering angles and diverges at $\theta\to0$. Overall, the standard semi-classical approach reviewed in this appendix is inferior to the MQCT treatment proposed in this paper, and from our point of view is not particularly useful (except Eq. (A6), used to compute the scattering phase $\delta_l$).

In the case of a single branch, i.e., outside of the rainbow point, in the classical scattering regime, one can substitute

$$f(\theta)=\frac{\sqrt{l_0}\,|a(l_0)|}{k\sqrt{\sin\theta\frac{\partial\Theta(l_0)}{\partial l}}}\exp\left\{i\left(-\int_{\infty}^{l_0}\Theta(s)ds-\left(l_0+\frac{1}{2}\right)\Theta\right)\right\} \tag{A14}$$

into Eq. (20), which yields classical expression for differential cross section:

$$\frac{d\sigma(\theta)}{d\Omega}=\frac{l_0\,|a(l_0)|^2}{k^2\sin\theta\left|\frac{\partial\Theta(l_0)}{\partial l}\right|}. \tag{A15}$$

In the body of the paper we called this version a pseudo-classical cross section, since the expression itself is classical, but the input data for probability $|a(l)|^2$ and the deflection function $\Theta(l)$ are obtained from MQCT calculations.

[1]A. Semenov and D. Babikov, J. Chem. Phys. **139**, 174108 (2013).
[2]G. D. Billing, Comp. Phys. Rep. **1**, 239 (1984).
[3]G. D. Billing, *The Quantum-Classical Theory* (Oxford University Press, 2002).
[4]M. Ivanov and D. Babikov, J. Chem. Phys. **134**, 144107 (2011).
[5]A. Semenov, M. Ivanov, and D. Babikov, J. Chem. Phys. **139**, 074306 (2013).
[6]A. Semenov and D. Babikov, J. Chem. Phys. **138**,164110 (2013).
[7]M. Ivanov and D. Babikov, J. Chem. Phys. **134**, 174308 (2011).
[8]M. Ivanov and D. Babikov, J. Chem. Phys. **136**, 184304 (2012).

[9]M. Ivanov and D. Babikov, Proc. Natl. Acad. Sci. U.S.A. **110**, 17708 (2013).
[10]G. D. Billing, J. Chem. Phys. **57**, 5241 (1972).
[11]J. Loreau, P. Zhang, and A. Dalgarno, J. Chem. Phys. **135**, 174301 (2011).
[12]A. Mack, T. K. Clark, R. C. Forrey, N. Balakrishnan, T.-G. Lee, and P. C. Stancil, Phys. Rev. A **74**, 052718 (2006).
[13]N. Balakrishnan, M. Vieira, J. F. Babb, A. Dalgarno, R. C. Forrey, and S. Lepp, Astrophys. J. **524**, 1122 (1999).
[14]J. B. Delos, W. R. Thorson, and S. K. Knudson, Phys. Rev. A **6**, 709 (1972).
[15]P. McGuire and D. J. Kouri, J. Chem. Phys. **60**, 2488 (1974).
[16]J. Ross, "Molecular beams," Adv. Chem. Phys. **X**, 75 (1966).
[17]M. Abramowitz and I. Stegun, *Handbook of Mathematical Functions with Formulas, Graphs, and Mathematical Tables* (Dover, New York, 1965).
[18]E. L. Degl'Innocenti, *Polarization in Spectral Lines* (Springer, 2006).
[19]See http://physics.bk.psu.edu/sigma/index.html for full quantum results of R. Forrey.
[20]R. Conte, B. Fu, E. Kamarchik, and J. M. Bowman, J. Chem. Phys. **139**, 044104 (2013).
[21]J. M. Bowman and S. C. Park, J. Chem. Phys. **77**, 5441 (1982).
[22]D. E. Manolopoulos and M. H. Alexander, J. Chem. Phys. **97**, 2527 (1992).
[23]M. H. Alexander, C. Rist, and D. E. Manolopoulos, J. Chem. Phys. **97**, 4836 (1992).